Journal of Experimental Marine Biology and Ecology 467 (2015) 52–64

Contents lists available at ScienceDirect

Journal of Experimental Marine Biology and Ecology

journal homepage: www.elsevier.com/locate/jembe

Impact of sediment grain-size and biofilm age on epipelic microphytobenthos resuspension

Martin Ubertini [a,*], Sébastien Lefebvre [b], Christiane Rakotomalala [a], Francis Orvain [a]

[a] Université de Caen Basse-Normandie, UMR BOREA "Biologie des ORganismes et Ecosystèmes Aquatiques" (MNHN, UPMC, UCBN, CNRS-7208, IRD-207), Caen, France
[b] Université de Lille1, UMR CNRS 8187 LOG "Laboratoire d'Océanologie et Géosciences", Station Marine de Wimereux, Wimereux, France

ARTICLE INFO

Article history:
Received 7 July 2014
Received in revised form 26 December 2014
Accepted 11 February 2015
Available online 22 March 2015

Keywords:
Microphytobenthos
Erodimeter
Resuspension
Biofilm
Extracellular polymeric
Substances
Sediment

ABSTRACT

Intertidal zones are dynamic areas, where tidal currents and wind-induced waves are responsible of resuspension of the sediment and associated microphytobenthos (MPB). Sediment composition (mud–sand mixtures) and MPB biofilm age are two major components involved in resuspension of epipelic microphytobenthos in muddy areas. However, their relative role in resuspension phenomenon must be better understood in controlled conditions. In this study, three mud–sand mixtures (Pure mud M1, 75% mud/25% sand M2 and 50% mud/50% sand M3) were tested with an epipelic MPB biofilm of different ages (3, 6 and 9 days after inoculum) using an erodimeter flume. The biofilm biomass, physiological state, photosynthetic parameters and Extracellular Polymeric Substances (EPS) were surveyed as well as water content and ammonium concentration in the sediment. Chl a content and Suspended Particular Inorganic Matter (SPiM) erodability differed between treatments, biofilm being able to be eroded before sediment when it is well constituted (especially in pure mud M1). Between day 3 and day 9 of culture, biofilm age did significantly affect critical thresholds for Chl a erosion and sediment resuspension for mud–sand mixtures (M2 and M3). Sediment resuspension seemed to be also driven by physical constraints like differential compaction and vertical sand segregation as a function of mud content. Indeed, grain-size was the main factor involved in MPB resuspension phenomenon, with an optimum reached near a equilibrate ratio between mud and sand (50% mud–50% sand). Proteins of the EPS bound fraction (extracted with dowex resin) appeared to have a critical role in the pioneering stages of biofilm installation, allowing its formation in a less favorable environment caused by sand enrichment (mixtures M2 and M3). This effect of bound EPS must be mediated by an increasing cohesion and lowering sediment permeability. Carbohydrate content of the bound EPS fraction was directly related to the sediment (SPiM) erodability, independently from mixture type or biofilm age.

1. Introduction

Macrotidal estuaries are open ecosystems subject to hydrodynamic processes such as wind induced waves and currents generated by tidal rhythm. The stress generated by these physical factors results in a resuspension of the sediment and associated microphytobenthos (de Jonge and van Beusekom, 1995). Microphytobenthic communities inhabiting cohesive sediments are mainly constituted of epipelic benthic microalgae – dominated by diatoms in intertidal mudflats (Smith and Underwood, 1998) – and are able to migrate vertically through the sediment top layer, according to a chronobiological rhythm (Mitbavkar and Anil, 2004). Tidal cycle and light are main factors explaining the migration of epipelic diatoms (Perkins et al., 2001; Blanchard et al., 2004; Mitbavkar and Anil, 2004), migration being mediated by the excretion of carbohydrate-rich heteropolymers called exopolymeric substances (EPS). EPS secretion by epipelic microphytobenthos is under control of abiotic factors such as light (Staats et al., 2000a) and nutrients (Staats et al., 2000b), and there is direct metabolic pathway between photosynthesis and secretion of colloidal EPS (Underwood and Smith, 1998). EPS are also able to stabilize the sediment by limiting the erosion of the latter (Friend et al., 2008; Grant et al., 1986; Holland et al., 1974; Paterson, 1989; Smith and Underwood, 1998, 2001). This microphytobenthos (MPB) biostabilisation of sediment surface is variable upon time, since MPB has its own dynamic and growth cycle. Combination of tidal cycles (McKew et al., 2011), day/night cycles (Cartaxana et al., 2011), biofilm age (Sutherland et al., 1998) and biomass lead to different physiological states of microalgae, thus influencing the sediment erodibility.

The biomass of MPB on intertidal flats is driven by (i) exportation processes such as grazing and resuspension, (ii) factors affecting growth rate and/or health of the MPB such as light, temperature or nutrients and (iii) sediment grain-size, with interaction with both previously mentioned factors (resuspension, nutrient availability). All these factors are drastically regulated by the respective contribution of sand and mud

* Corresponding author at: 3 rue du Prêche, 50170 Pontorson, France. Tel.: +33 633383047.
E-mail address: martin_ubertini@hotmail.com (M. Ubertini).

http://dx.doi.org/10.1016/j.jembe.2015.02.007
0022-0981/

proportion (Orvain et al., 2012; Van de Koppel et al., 2001). When factors responsible for MPB losses from sediment (resuspension, grazing) are removed, the growth of the biofilm is known to follow a logistic curve until a maximum value reached at the biotic capacity of the local environment (Blanchard et al., 2001; Orvain et al., 2003a, 2003b). The number of days necessary to reach the biotic capacity differs according to the authors, and has been modeled by Wolf (2007) with an initial lag phase of about 3 days, followed by an exponential growth phase until a pseudo-steady state "mature" phase after approximately 13 days. The physiological state of the biofilm is assumed to change as a function of the biofilm age (Sutherland et al., 1998). Photosynthetic capacity and light use efficiency has been shown to decrease with increasing biofilm development (Morris, 2005; Serôdio et al., 2005), and EPS are more secreted in the late phase of the biofilm development caused by overflow metabolism in case of nutrient limitation (Orvain et al., 2003a, 2003b).

Physical factors are decisive regarding sediment stability against biological ones. Sandy sediments are easily transported by haulage during bed-load transport and exported in the water column during strong hydrodynamic conditions. On the contrary, cohesive sediments resist to erosion but, in the case of harsh conditions such as strong swells, critical thresholds can be transcended leading to significant sediment massive erosion. Numerous experiments focusing on microphytobenthos mediation of sediment erodibility have been done in laboratory conditions, most of the time focusing on homogeneous sandy (De Brouwer et al., 2005; Friend et al., 2008; Lucas, 2003) or muddy sediments (Andersen and Pejrup, 2002; Droppo et al., 2007; Gerbersdorf et al., 2007; Orvain et al., 2004; Spears and Saunders, 2008; Stone et al., 2008; Tolhurst et al., 2003, 2006, 2008; Yallop et al., 2000). However, sand and mud can be intimately mixed in natural intertidal systems, and may exhibit a horizontal gradient, or can be layered in the bed (Le Hir et al., 2011). The mixture behaves mostly like pure sand, but there is a critical mud fraction (typically 30%), above which the mixture behavior is fully cohesive (Le Hir et al., 2011). Below this critical value, the mixture shear strength depends on the relative mud concentration as stated by Migniot (1989) and Waeles et al. (2008). In fact, if physical processes such as local hydrodynamic conditions are responsible for particle grain-size selection, a succession of vertical layers of sediment from different grain-size often occurs in nature. Moreover, biological processes such as bioturbation and sediment reworking can influence the particle mean-size, leading to modify the sediment vertical structure, therefore leading to bulk sediment mixtures (Krantzberg, 1985). As a consequence, intertidal ecosystems are often characterized by mud–sand mixed sediments, with a strong spatial heterogeneity from pure sand to pure mud (Orvain et al., 2012; Ubertini et al., 2012). These mixed sediments must be taken into account in both microphytobenthos development and material export to the water column by erosion processes. Erosion thresholds of sediment mixtures in relation with microbial indices have been studied in situ (Defew et al., 2003; Lelieveld et al., 2003; Ziervogel and Forster, 2006) or by modeling approaches (Le Hir et al., 2011; Paarlberg et al., 2005; Waeles et al., 2008), but rarely in controlled conditions. Van de Koppel et al. (2001) clearly put in evidence the positive effect of mud proportion on the biofilm growth. However, the combined effect of mud–sand proportion and microphytobenthic biofilm age has never been experimented to evaluate the contribution of these 2 factors in the response of sand, mud and chl a erodability.

The objectives of the study were to characterize: 1) the influence of grain-size on a MPB biofilm development within a controlled environment, 2) the tidal currents influence on both epipelic microphytobenthos and sediment resuspension, 3) the relative and interacting effects of sediment grain-size and biofilm age on this phenomenon. In order to do this, mesocosm biofilm cultures were controlled to assess different development stage of the biofilm by regulating emersion-immersion periods under a night and day light cycle.

2. Materials and methods

2.1. Experimental design

We used natural sand and mud sediments respectively coming from a beach located at Luc sur mer and a mudflat located in the Bay of Veys (Basse-Normandie, France). There were taken from the 10 top cm. The 2 stocks of sediment were left outdoors for 1 month in order to remove the bulk of the present MPB. In order to eliminate the macrofauna naturally present, the fresh sediments were sieved with water using a 1 mm mesh size, this mesh size being the minimal size allowing fine sediment to be sieved with the volumes we used. In order to remove most of the organisms ranging from 0.5 to 1 mm, sediments were unused for 1 month. Three cohesive sediment types (Fig. 1) were prepared: one of pure mud (100%, mixture M1) and two mud–sand mixtures (75% mud/25% sand and 50% mud/50% sand respectively mixture M2 and M3). For each of these mixtures, sediment was then dispatched in twelve cores (20 cm in diameter and a depth of 20 cm). The first upper cm was enriched with an epipelic MPB inoculum collected from a mudflat – with typical grain-size corresponding to M1 – located in the Orne estuary (WGS84, 49°16′17.41″N, 0°14′7.24″O) in Basse-Normandie during April 2011. It was collected by scratching the sediment surface. The biofilm was mainly composed of pennate diatoms including small *Navicula* sp. (length ~17 μm, >95% of total MPB), *Amphora* sp., *Pleurosigma* sp., *Niztschia* sp. and *Cylindrotheca closterium*. The core surface was then wreathed in order to be uniform as best as possible on the whole surface. The cores were placed in a tidal mesocosm able to simulate a high/low tide alternation every 6 h in order to simulate immersion and emersion phases. A night and day alternation (18 h/6 h) was applied with adapted neon lights, with a light intensity of 1600 μmol photons $m^2.s^{-1}$ (LUMINUX, 36 W Osram). The combination of light intensity and duration was chosen as a function of the photoperiod at the moment of the experiment (April). Each of these sediment series was tested during 3, 6 or 9 days continuous treatment, with a sub-sampling within cores allowing At days 3, 6 and 9, 4 sub-cores were sampled within each culture cylinder, of which 3 were dedicated to sediment and biofilm features analyses and 1 was dedicated to erosion experiments (see Fig. 2 for the experimental design drawing).

2.2. Pigment extraction and analyses

Sediment samplings within the experimental cores were performed at 3, 6 and 9 days at the beginning of diurnal emersion periods in order to access respectively the latency, growth and stationary phases of the biofilm (Orvain et al., 2003a, 2003b; Sutherland et al., 1998). The first upper cm of the sediment was sampled and mixed, and fresh sediments were weighted. This depth was chosen as the maximum depth for diatom vertical migration (Saburova and Polikarpov, 2003). After 3 days in an oven at 60 °C a weight measurement was also done to obtain the water content of the sediment. Microphytobenthos content was assessed by measuring the chlorophyll *a* (Chl a) content following the Lorenzen's method (Lorenzen, 1967). Chloropigments were extracted from 200 mg freeze-dried sediment subsamples with 90% acetone solution for 24 h at 4 °C in the dark. After centrifugation (5 min, 2000 *g*, 4 °C), fluorescence of the supernatant was measured using a TD-700 Fluorometer (Turner Design, USA) before and after acidification (HCl 0.3 M for 1 mL of supernatant). Total Chl a and pheopigment biomass were calculated according to Lorenzen equations. In order to avoid the dewatering over the emersion period (Perkins, 2003), water content and bulk density of the sediment were used to express the Chl a as a content per m^{-2}. Microphytobenthos physiological state measurements as well as photosynthetically active biomass measurements have been done using a Pulse Amplitude Modulation fluorometer (PAM, Walz-Mess und Regeltechnik, Deutschland, see Section 2.5).

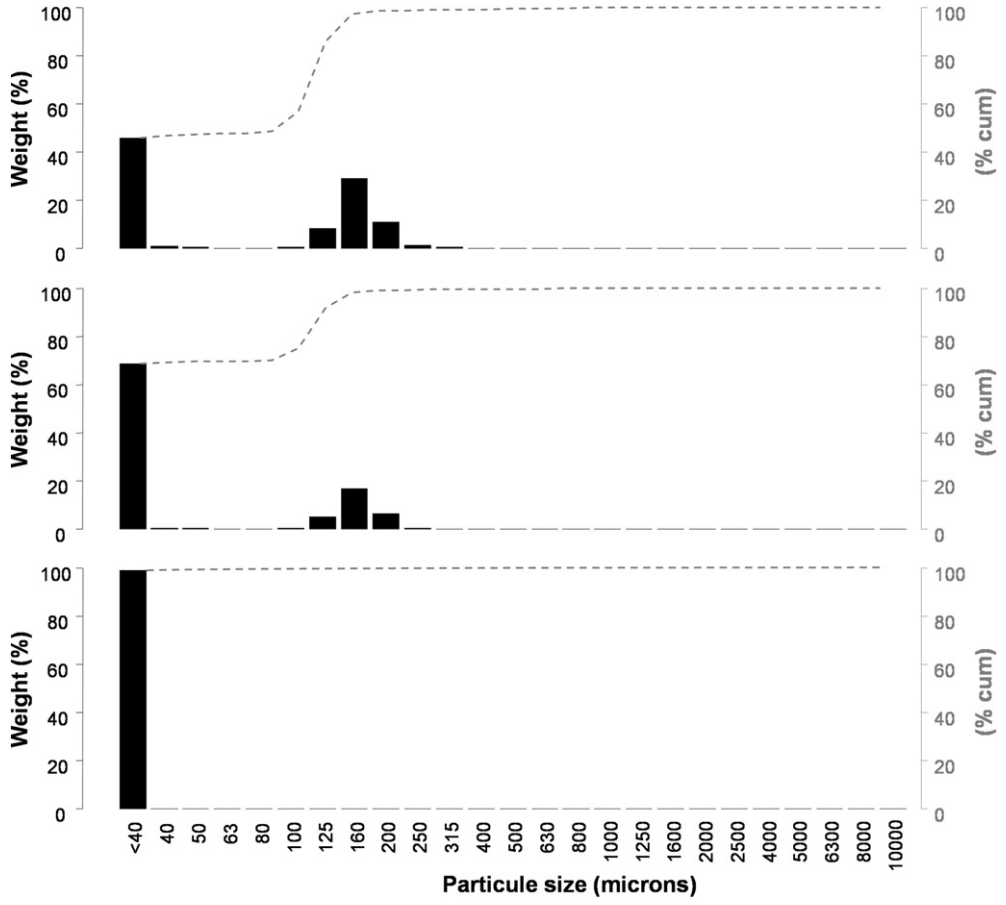

Fig. 1. Grain-size distribution of the 3 sediment mixtures used for the experiment.

2.3. EPS and NH_4^+ extraction and analyses

EPS extraction was done immediately after sampling and sediment mixing on unfrozen sediments (Takahashi et al., 2009). In order to obtain the colloidal EPS, a 20 mL fresh sediment subsample was mixed with 20 mL of Artificial Sea Water (ASW 30 Practical Salinity Units), agitated during 1 h at 4 °C in dark conditions and then centrifuged at 3500 *g* and 4 °C for 10 min. The supernatant containing **c**olloidal EPS was collected and stored at −20 °C. In order to extract the bound EPS fraction, a 20 mL of ASW and ~3 g of activated Dowex (Marathon C, activated in Phosphate Buffer Saline for 1 h in the dark) was added to the cap. The samples were mixed gently at 4 °C for 1 h in the dark and then centrifuged at 3500 *g* and 4 °C for 10 min. The supernatant containing bound EPS was collected and stored at −20 °C. The Dubois's method (Dubois et al., 1956) was applied to quantify the carbohydrate fraction with a using a UV-1700 Spectrophotometer (*Shimadzu, Japan*). The Bradford method (Bradford, 1976) was adapted to a luminometer LB940 Mithras (Berthold Technologies, U.S.A.) and permitted to quantify the proteic fraction of EPS. The content of carbohydrate and protein in EPS from 1st cm sediment were expressed in $mg.m^{-2}$ by using a conversion in the basis of the volumetric mass of sediment. The first sediment centimeter was partly sampled and centrifuged in order to measure the ammonium amount in sediment interstitial water following the Holmes fluorometric method (Holmes et al., 1999).

2.4. Rapid light curves (RLCs)

Variable chlorophyll *a* fluorescence was measured using a Pulse Amplitude Modulation (PAM) fluorometer including a PAM-control unit and a WATER-EDF-universal emitter-detector unit (Walz, Effeltrich, Germany) following the method of Lefebvre et al (2011). This apparatus is equipped with a modulated blue light (LEDs with maximum emission at 450 nm), which serves as the same light source for the measuring beam, and the actinic and saturating lights. Irradiances were calibrated against a quantum sensor (LI-COR Li 190) at a distance of 5 mm. A sediment mini-core (2 cm in diameter and depth) was taken from the mesocosm culture and place in a dark box where the PAM fiber optic probe is placed at a constant depth of 5 mm from the sediment surface. Replicated mini-core location was chosen randomly within the sediment cores from the mesocosm culture. An estimation of the effective quantum yield of PSII (ΔF/Fm′) was measured few seconds after positioning the probe (Serôdio et al., 2008), by applying a saturating flash of 800 ms at around 3800 µmol photons $m^{-2}.s^{-1}$. RLCs were then constructed by exposing the MPB biofilms to eight steps of increasing irradiance without prior dark acclimation (around 70, 100, 150, 220, 310, 430, 710, 1000 µmol photons $m^{-2}.s^{-1}$). The duration of the irradiance steps was 30 s. Each experimental day, four replicates of each treatment were randomly performed in turn. The relative electron transport rate (rETR) was calculated at each level of irradiance, as the product of the effective quantum yield of PSII and the delivered irradiance: $rETR = \Delta F/Fm' \times E$. The minimum level of fluorescence (F_{o5}) was conveniently estimated after 5 min of dark acclimation at the end of the RLCs and then immediately followed by the estimation of the maximum quantum yield (F_{v5}/F_{m5}). As F_{o5} was measured at different photomultiplicator gains, the relative level of fluorescence were standardized at a level of PMgain = 5 using using a solid chl a standard. F_{o5} is used as an estimate of the photosynthetically active biomass in the top layers of the sediment (see Orvain et al., 2014, for details). The light response of rETR curves (rETR/E) was constructed using the model of Eilers and Peeters (1988). This model allowed us to

estimate the maximum rETR ($rETR_{max}$), which is the asymptote of the curve; the maximum light use efficiency (α), which is the slope at the beginning of the curve; and the light saturation coefficient ($E_K = rETR_{max}/\alpha$). Curve fitting was achieved using the downhill simplex method of the Nelder–Mead model, and standard deviation of parameters was estimated by an asymptotic method. All fittings were tested by analysis of variance ($p < 0.001$), residues being tested for normality and homogeneity of variance, and parameter significance by Student's *t*-test ($p < 0.05$). All the data treatment (scatter minimisation) and associated statistics were coded under MATLAB R2009b.

2.5. Erosion experiment

Erosion tests were executed using the ERODIMETER, a small-scale (1.20 m long, 8 cm wide and 2 cm high) straight transparent flume (Le Hir et al., 2007). For each sampling day, 4 cores were sampled preserving their surface integrity and were placed by 2 into the flume (2 experiments per condition). Each sediment sample was directly transferred from a cylindrical core to the bottom of the flume (Le Hir et al., 2008). Sediment cores have been submitted to a controlled flow in a 15 L filtered sea water close-circuit. After an initial flow during 15 min, an increasing flow was applied every 5 min (32 successive levels) using a pump with a variable frequency drive (Fig. 1). The induced bed shear stress has been calibrated by eroding well-sorted non-cohesive particles and direct confrontation to the Shields threshold criterion (Guizien et al., 2012; Le Hir et al., 2007). Flow discharge and differential pressure were also continuously recorded between upstream and downstream the sediment samples. The bed shear stress (BSS) was calculated following the method by Guizien et al. (2012) to take into account for the differences in bottom roughness between treatments by using a differential pressure gradient. The erosion parameters were measured by estimating the fine particle amounts in the water using a nephelometric probe (NTU), and estimating the Chl a biomass in the water using a fluorescence probe.

2.6. Resuspended material sampling

The concentrations of Suspended Particle inorganic Matter (SPiM) were used do determinate the erosion features of the different conditions. At 4 frequency levels corresponding to 0.166, 0.582, 1.195, 1.852 Pa (friction force), a duplicated water volume of 0.5 L water was sampled during the erosion experiment in order to evaluate Chl a biomass and SPiM concentration (see 2.4.). In order to determine the SPiM concentration, two subsamples per level were sieved and passed through pre-combusted weighed and dried glass-fiber filters (Whatman GFC), washed with distilled water to avoid salt errors, packed in petrislides (Millipore, USA), and immediately stored at −20 °C before analyses. The filters were dried in an oven at 50 °C during 72 h, and then during 4 h at 450 °C to estimate the organic content of resuspended material concentration (SPoM). From the Total resuspended material (SPM) and SPoM, the Inorganic fraction was calculated (SPiM). For water column Chl a, two subsamples were sieved and passed through a glass-fiber filter (Whatman GFC), fold and put in a tube at −20 °C before analyses. The Chl a content of the sediment was extracted in 90% acetone during 24 h in the dark at 4 °C. After short centrifugation (10 min, 3000 *g*, 4 °C), the chlorophyll extracts were measured on a Turner Designs TD 700 fluorometer (USA) following the method of Lorenzen (1967) and expressed as content ($\mu g.m^{-2}$ sediment).

2.7. Mathematical treatment of erosion kinetics

Fluorescence data for water chl a were calibrated upon filtered Chl a concentration to be converted upon the basis of the most appropriate calibration curve (Fluorescence versus Chl a). Fluorescence data were also corrected to account for the dilution effect of sampling process, since 2 L of water was sampled for filtration at 4 successive steps all along the erosion experiment and the quantity of filtered water was added to adjust the whole volume in the system. The rate of erosion of the chl a was deduced from the time derivative of the fluorescence curve, after calibration and correction for dilution effects. The mass of eroded Chl a was computed as the product of Chl a concentration ($\mu g.L^{-1}$) by the water volume (15 L), divided by this sediment area $2 \times (\pi \times 0.045)$ in m^2. Among the 18 experiments, data of 1 experiment was not considered because of equipment failure. Erosion kinetics were analyzed to determine the critical threshold for erosion by determining the intersection point with X-axis when drawing a regression line between Chl a (averaged for each flow step) versus log ($U^* + 1$): chl $a = A \times \log(U^* + 1) + B$, where U^* is the shear velocity (in $m.s^{-1}$). The critical value of BSS for erosion is calculated by converting the one of shear velocity u^* and by using the usual formulation between u^* and τ_f, the BSS: $\tau_{f\,crit} = \rho \cdot \mu_{crit}{}^2$. The best regression line was retained and erosion rate was determined by considering only flow steps, for which the critical BSS was reached. For the concerned data, the rate of erosion was deduced from the time derivative of the Chl a curve, after calibration. Erosion rates ($g.m^{-2}.s^{-1}$) were assessed at each step (after erosion incipient point) as the slope between the eroded chl a (i.e chl a converted in $\mu g.m^{-2}$) and Δt the time interval between each chl a concentration record (1 s). The averaged erosion rate was calculated from the different values calculated per step.

Because nephelometric probe was less sensitive in the first erosion levels and problems caused by the presence of sand in the water at high flow regimes, turbidity data were not used for estimation of resuspension fluxes. Sediment erodability parameters were estimated by following the same procedure than for chl a but calculations relied on the filters SPiM data. Erosion kinetics calculation and representation were done using Matlab (Mathworks, USA).

2.8. Statistical tests

GLM were performed using Minitab (Minitab inc., USA) in order to compare the results regarding to the sampling day (3 modalities: day 3, day 6, day 9) and sediment mixture type (3 modalities: M1, M2, M3) and their interactions followed by post-hoc Tukey tests. Data were log-transformed when normality of distribution could not be satisfied. Principal components analyses (PCA) using the R package ADE4 (R-project) were used to identify the global effect of both mixture type and sampling day on sediment resuspension. For PCA data were centered and scaled.

3. Results

3.1. Diatom related biofilm analyses

Results showed a significant difference between the benthic chl a concentration as a function of the sediment mixture and the sampling day. There was also a significant effect of the interaction between the 2 factors (Table 1, Fig. 3A). The intermediate mixture (M2) was characterized by a significant higher content than the 2 other mixtures at day 9 (Fig. 3A). The index of Photosynthetically Active Biomass (PAB as estimated by F_{05}) was found to differ regarding to the sampling date within each sediment mixture type (significant interaction, Table 1, Fig. 3B). The highest values of 320–360 (relative units) were found for the intermediate mixture (M2), at day 9 and at day 3 for pure mud (M1) and intermediate mixture (M2) (Fig. 3B). F_{05} remained almost constant in M3 (a slight increase was registered on day 9) and below values of M1 and M2. The physiological state of microalgae (indicated by the maximum quantum yield: *Fv5*/*Fm5* ratio) varied with mixtures and date as well as their interaction (Table 1), with a decrease for all mixtures between day 3 and 9 (Fig. 3C). M1 showed better physiological state than M2 and M3. The model of Eileers and Peters was generally well appropriate to describe RLC curves (Fig. 4).

Table 1
F-values of general linear models testing the relative effects of the mixtures (3 modalities M1, M2, M3) and biofilm development (3 modalities 3, 6, 9) as well as the interactions between these 2 factors. Response variables were sedimentary descriptors, erodibility characteristics and photosynthetic parameters. Significance of the statistical results is given by asterisks. Results of the post-hoc tests (Tukey) are given in Figs. 3, 5 and 7.

Variable	Mixture	Biofilm development	Mixture * sampling day
τ_{crit} (Chl *a*)	25.2***	0.5	2.5
Flux (Chl *a*)	3.2■	0.8	0.9
τ_{crit} (SPiM)	0.2	0.2	0.7
Flux (SPiM)	1.7	0.3	0.7
Prot. Coll. EPS	45.3***	3.3■	6.3***
Prot. Bnd. EPS	38.0***	28.8***	0.8
Carb. Coll. EPS	24.0***	3.3	1.4
Carb. Bnd. EPS	56.5***	27.9***	7.4***
Water content	120.8***	7.3**	3.9*
Benthic Chl *a*	24.0*	8.1**	2.2■
F_{05}	4.6*	5.6**	3.14**
F_{v5}/F_{m5}	45.93***	92.7***	15.2***
$rETR_{max}$	2.41	0.33	2.42■
α	1.7	10.9***	2.4■
E_K	3.2■	1.6	2.2■

■ $p < 0.1$.
* $p < 0.05$.
** $p < 0.01$.
*** $p < 0.001$.

The mixture type had no significant effect on α parameter, but the latter decreased as a function of the biofilm development stage for M2 and M3, remaining constant for M1 (Fig. 3D, Table 1). The decrease of α with time was more pronounced for M3 (Fig. 4). Mixture type had a significant effect on $rETR_{max}$, M3 being characterized by lower values. Biofilm age had no significant effect on $rETR_{max}$ (Fig. 3E). Mixture type had a significant effect on the parameter E_k, this parameter decreasing with higher proportion of mud in the mixtures from M3 to M1 (Fig. 3F).

Pore water content varied as a function of mixture type (Table 1), increasing with the mud proportion increase (from M3 to M1). Pore water content stayed stable within each mixture regarding to the day factor excepted for the mud condition (M3), which significantly decreased at day 9 (Fig. 5A). There was an increase in NH_4^+ porewater concentration between days 6 and 9 for pure mud (M1, Fig. 5B). Intermediate mixture (M2) showed a slight decrease of NH_4^+ concentration between days 3 and 6 reaching a near zero concentration at day 6, whereas the sandier mixture (M3) showed null concentrations or concentrations under the limit of detection of the method for all dates. Carbohydrates were 1000 times more abundant than proteins for both bound and colloidal fractions of EPS (Fig. 5). Carbohydrate content of colloidal EPS fraction differed significantly as a function of sediment mixture (Table 1), the amount of EPS increasing with the mud fraction M1 (Fig. 5C). These EPS did not vary significantly nor with date neither with interaction between date and sediment mixture (Table 1). For the bound EPS fraction, the carbohydrate content varied significantly as a function of both mixture and time as well as their interaction (Table 1), with a larger amount for M1 than for M2 and M3 (Fig. 5D). However the amount of carbohydrate from bound EPS did not differ significantly at day 9 for all mixtures, with a significant effect of interaction between the 2 factors (Table 1). Indeed there was also a change in the carbohydrate amount of bound EPS as a function of date, with a significant decrease in the mud between days 3 and 6 and an increase for the intermediate (M2) and sandier mixtures (M1) between days 6 and 9. M2 and M3 did not show significant differences between dates. The amount of carbohydrate from the colloidal fraction did not differ significantly at day 9 for all mixtures. The protein component of colloidal EPS

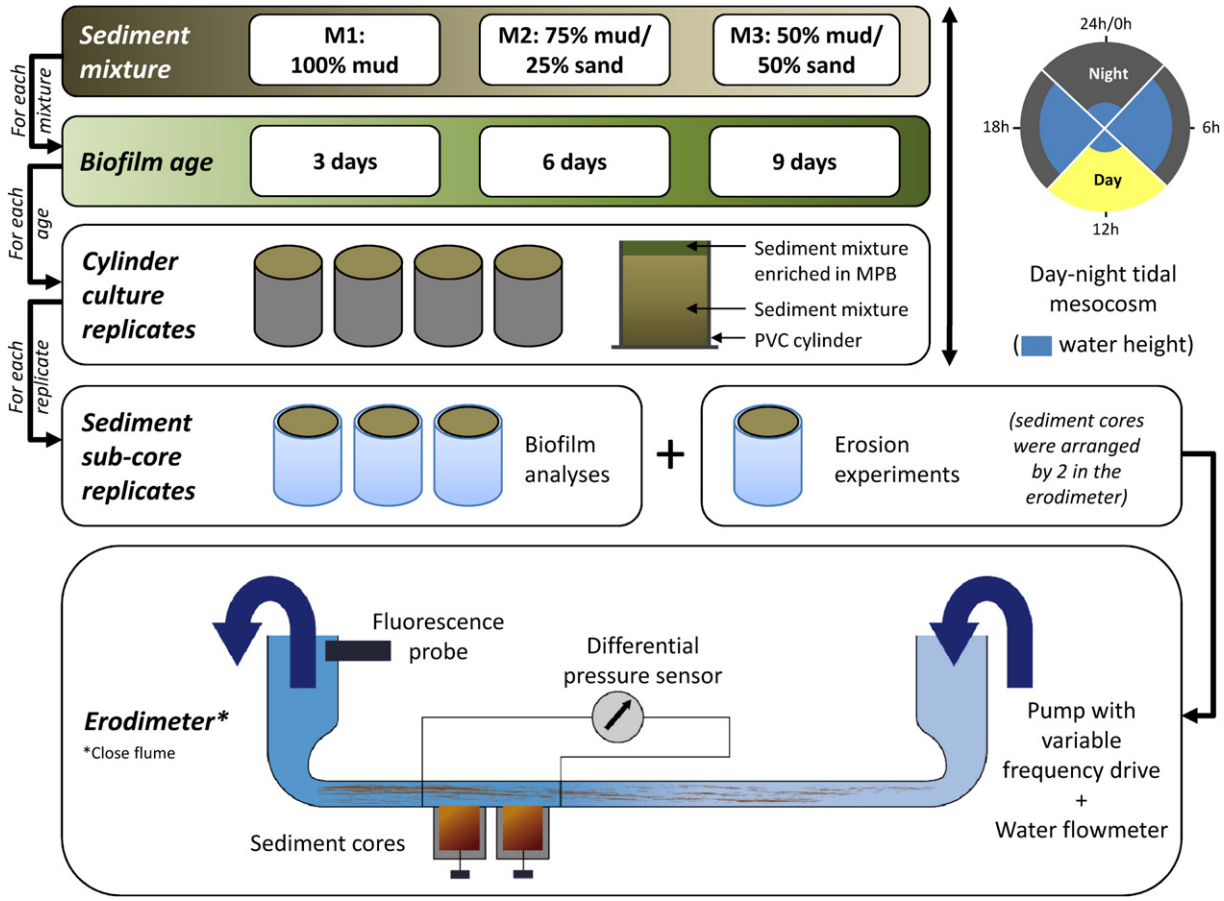

Fig. 2. Experimental design.

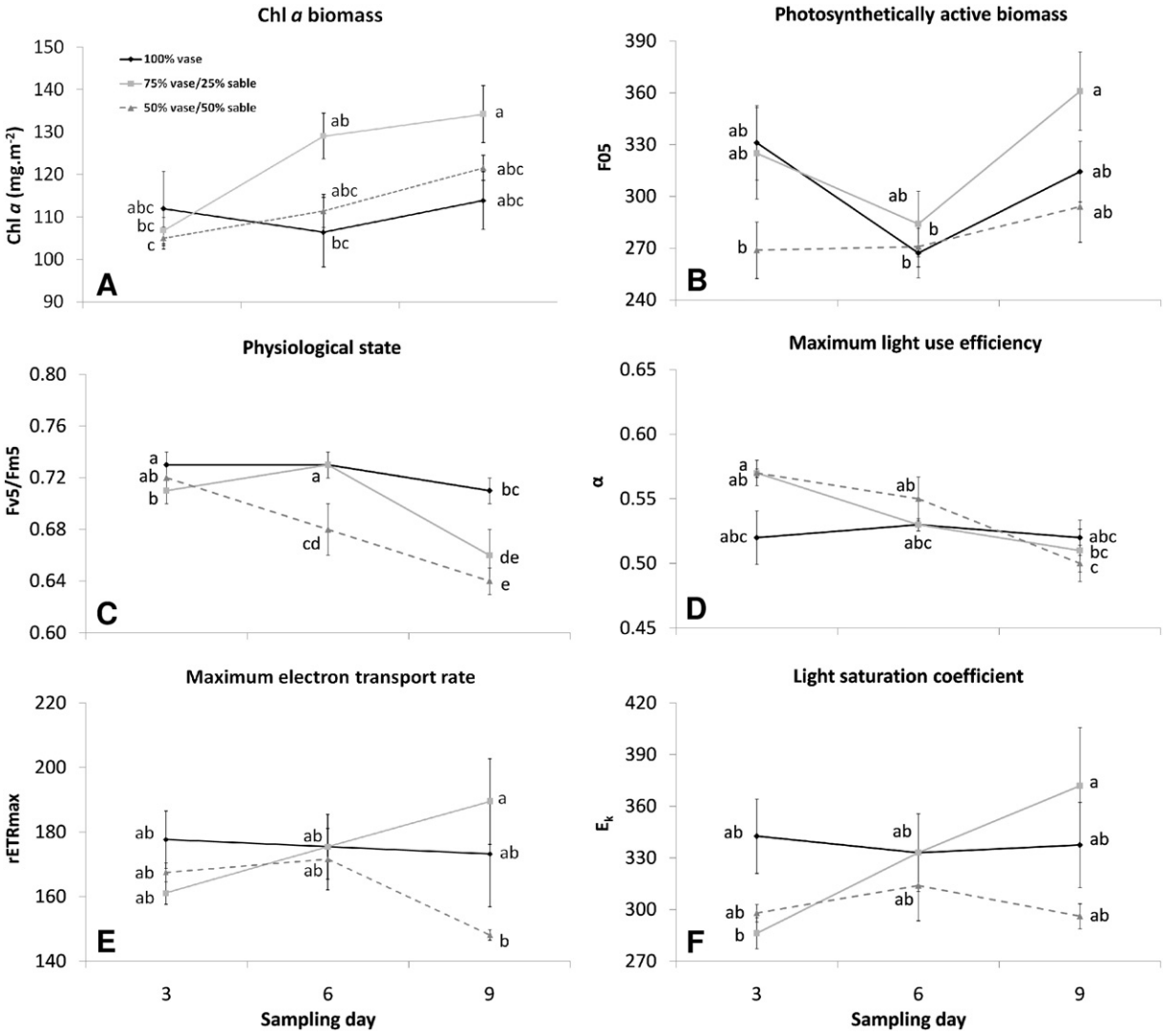

Fig. 3. Biofilm related variables measured at the sediment core surfaces for the different sampling days. A: microphyotbenthos (MPB) content as measured by Chl *a* biomass; B: Photosynthetically active biomass (PAB) of the biofilm as estimated by the minimum level of fluorescence after 5 min in the dark (F_{05}); water content, both in the top first cm of the sediment. C: physiological state of the biofilm as estimated by the maximum quantum yield (F_{v5}/F_{m5}). D: maximum light use efficiency (α, initial slope of the rETR/E curves); E: maximum electron transport rate (rETRmax the asymptote of the curves); F light saturation coefficient (EK = rETRmax/α). Letters indicate groups after post hoc test procedures (see Table 1 for further details).

(Fig. 5E) varied significantly depending on the mixture (Table 1), with a higher proportion in M1 (mud) than for M2 and M3 in which the difference was not significant at day 3 and day 6, day 9 being characterized by a higher content for the intermediate mixture (M2). The protein content of bound EPS (Fig. 5F) varied significantly depending on the mixture, but surprisingly M2 showed the highest values. This amount also changed significantly as a function of date, day 3 being the lowest.

3.2. Effect of biofilm age and grain-size on erosion

Erosion kinetics of chl a concentration (Fig. 6) showed relatively low differences between replicates, excepted for the sandier mixture (M3), with M3D6 and M3D9 showing a low chl a erosion while high erosion fluxes were obtained for the other replicate. Chl a erosion rates were clearly more subject to variability than critical thresholds. Erosion can be characterized by 2 different types. Type I erosion can be detected by an achievement of chl a kinetic to an asymptotic plateau after less than 5 min at a given bed shear stress, for unconsolidated sediment. Type II erosion corresponds to mass erosion of consolidated sediments. For the pure mud, there was type I erosion decreasing before the end of kinetics or reaching a second state of erosion corresponding to type II erosion. The intermediate mixture was characterized by the 2 types or erosion at day 3 and 9 but only type I erosion on day 6. The extent of variation was similar for the pure mud and intermediate mixture interms of chl a erosion. The sandier mixture was characterized by type II erosion whatever the bed shear stress. Chl a erosion was characterized by higher critical erosion threshold as a function of the sand content of the mixtures, and higher erosion rates, when the sediment was enriched in sand (Table 1, Fig. 7). Biofilm age had neither effect on erosion critical threshold, nor effect on erosion rates (Table 1).

For the SPiM, there were no significant differences between the erosion critical thresholds in terms of grain-size or biofilm age (Table 1). These two parameters were neither related to the SPiM erosion fluxes (Table 1). However, the interaction of these two factors did affect significantly both erosion critical thresholds and erosion flux associated to SPiM (Table 1). At day 3, $\tau_{crit(SPiM)}$ and erosion flux associated to SPiM were higher at day 3, for the muddier mixture. At day 9, these two parameters were higher for the 2 mud–sand mixtures (M2 & M3).

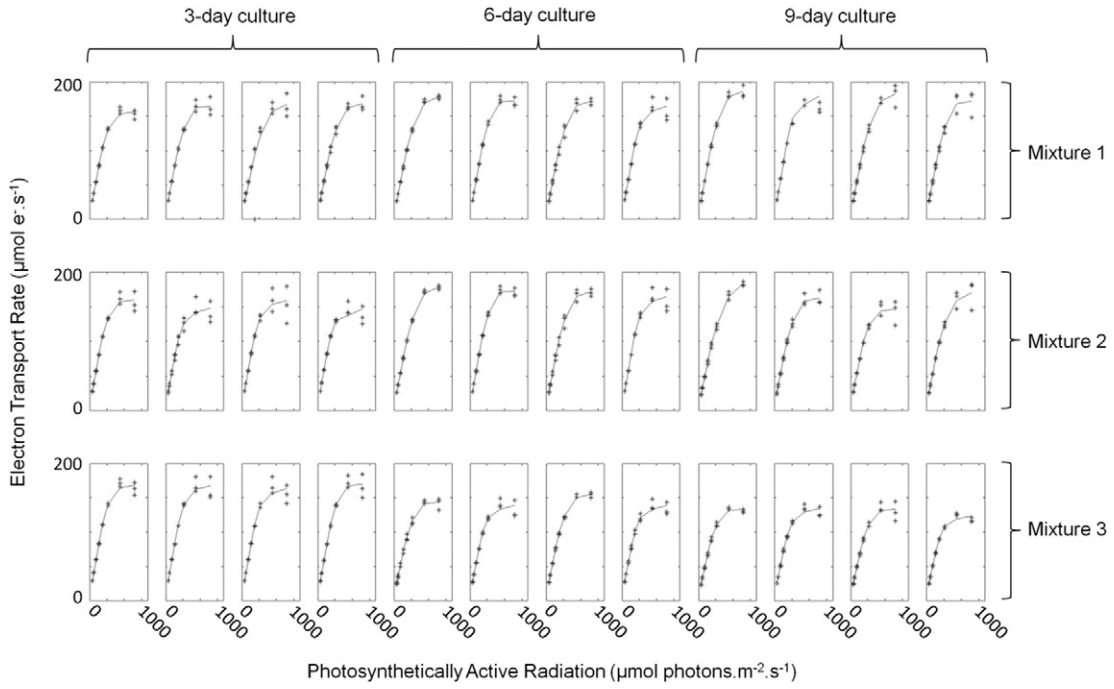

Fig. 4. Rapid light response curves (RLCs) of the relative electron transport rate (rETR) of sediment core microphytobenthos (MPB) biofilms grown under 1600 µmol photons $m^2.s^{-1}$ intensity during low-tide exposure period at days 3, 6 and 9 for the 3 sediment mixtures. RLCs were run with 30-s light step increments. Observations black points, continuous line = fitting of the Eilers and Peeters (1988) model.

3.3. Synthesis of the analyzed parameters influence on erosion

A PCA was applied to sediment variables and erodability parameters (Fig. 8), and only the two first components were retained, explaining 53.47% of the total inertia. The correlation circle (Fig. 8A) showed that Chl a τ_{crit} and erosion rate were well represented on the 1st axis, anti-correlated with EPS fractions, $NH4^+$ and water content of the sediment, this axis explaining 36.10% of the total inertia. Generally speaking, the porewater of the mud (M1) was higher, with higher ammonium concentration and EPS secretion, and the chl a biomass was easily eroded, despite consolidation. SPiM τ_{crit} and Chl a biomass were well represented on the 2nd axis – explaining 18.02% of the total inertia – anti-correlated to the ratio *Fv/fm* and α. The mud mixture is thus less erodible regarding sediment, with high chl a biomass. Both F_{05} and rETRmax were poorly represented on the two first components. The scatter-plot of individuals (Fig. 8B) showed a clear difference between the experimental conditions, which were merged into three groups corresponding to the 3 tested mixtures, discriminated on the first axis, and 3 sub-groups, corresponding to the biofilm age, discriminated on the second axis. Pure mud appeared to be mostly characterized by higher values than mud–sand mixtures for all EPS extracts.

4. Discussion

The objectives of the study were to characterize the tidal currents influence on both epipelic microphytobenthos and sediment erodbility. We were interested in highlighting the relative and interacting effects of sediment grain-size and biofilm age on this phenomenon.

4.1. Development and physiological state of the biofilm

There was a slight effect of mixture on epipelic chl a content and photosynthetically active biomass of the sediment, the intermediate sediment mixture (75% mud/25% sand, M2) being characterized by a higher chl a content than the 2 other tested mixtures (100% mud, M1 and 50% mud/50% sand, M3). Under natural conditions, cohesive sediments are known to be colonized by epipelic diatoms (Admiraal et al., 1994). On the contrary, in regions characterized by higher hydrodynamic stress, epipsammic species live attached to sediment grains. In this study, the diatom inoculum that was added to the sediment mixture came from an estuarine mudflat and they were mainly composed of epipelic species assemblages. Our results show that epipelic diatom communities were adapted to mud–sand mixtures with moderate sand fraction in terms of biofilm growth. A higher permeability of the sediment reduces the accumulation of regenerated nutrients in the pore water (Ehrenhauss et al., 2004), thus microphytobenthos development could be limited in the sandier mixture, even if the latter was still a cohesive sediment. This observation is in line with observations made by van de Koppel et al. (2001).

The absence of NH_4^+ between day 6 and 9 for the intermediate mixture (M2) and its absence for the sandier mixture (M3) probably lead to a nutrient limitation, lowering the MPB biofilm physiological state (decrease of the maximum quantum yield: F*v5/Fm5*) for M2 and M3 (Parkhill et al., 2001). Ammonium limitation could be also due to its higher consumption. Photobiology of the biofilm is driven by nutrients and light. Light was a controlled factor assumed to be constant between treatments, Chl a content and F_{05} being roughly the same. Light attenuation is higher in mud compared to sand (Jesus et al., 2005; Serôdio, 2003), thus available light for MPB may have varied between our 3 mixture conditions. The decrease of α and rETRmax as a function of time was more pronounced for the sandier mixture (M3), this decreasing co-variation being typical of a nutrient limitation (Behrenfeld et al., 2004) and especially ammonium porewater concentration (Table 1). On the contrary, M2 showed a typical photoacclimation with an increase in the light saturation coefficient E_k, resulting from an increase in rETRmax while α decreased (MacIntyre et al., 2002), leading us to conclude for no nutrient limitation at this stage. As for M1, photosynthetic capacity and physiological state stayed stable during the course of the experiment indicating quasi steady state conditions.

Colloidal EPS (in terms of carbohydrate as well as protein composition) confirmed the interacting effects of sand enrichment (from M1 to M3) and biofilm age affecting the photobiology of the

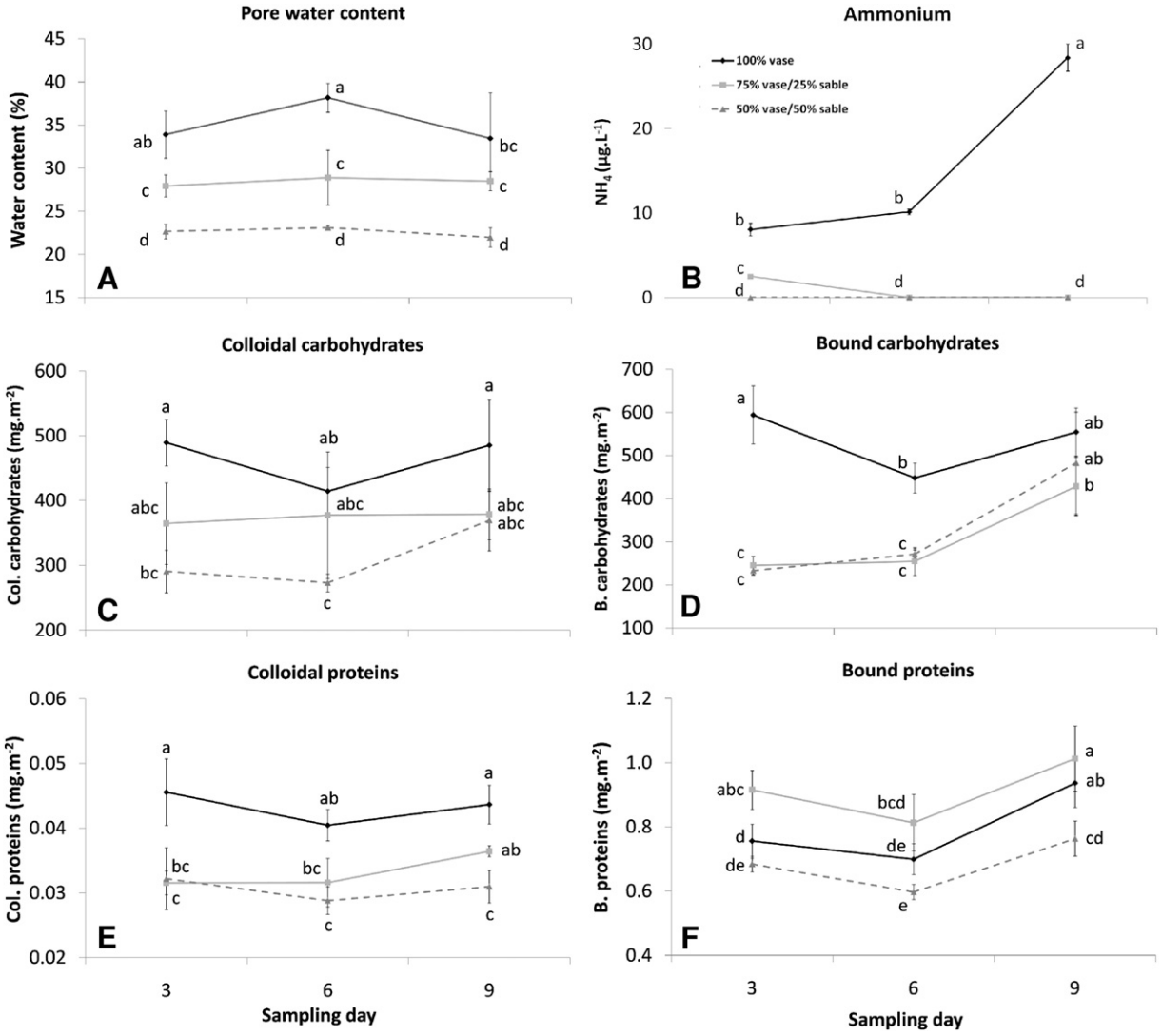

Fig. 5. Pore water content, ammonium and exopolymeric substances (EPS) fractions measured in the first top cm of the sediment core for the different sampling days. A: pore water content; B: NH_4 pore water content; C: carbohydrate content of colloidal EPS; D: carbohydrate content of the bound EPS; E: protein component of colloidal EPS; F: protein content of bound EPS. Letters indicate groups after post hoc test procedures (see Table 1 for further details).

latter. For the pure mud (M1), the level of secreted colloidal EPS remained high all along the experiment while the sandiest mixture (M3) presented the lowest colloidal EPS amounts. Even though EPS losses must be amplified in sand – because of a higher EPS hydrolysis and/or leaching – benthic diatoms must also secrete less colloidal EPS in sand, likely because of low chl a content as well as a decrease of photosynthesis efficiency caused by a nutrient stress in the sandier mixture (M3). Smith and Underwood (1998) clearly showed that there is a direct linkage between photosynthesis and the metabolic pathway of colloidal EPS secretion. Contrary to Orvain et al. (2003a, 2003b) or Staats et al. (2000b), no overflow metabolism did occur, even in the pure mud (maybe because the diatom culture was not long enough). There is also a possibility that the overflow metabolism observed by these authors was in fact biased by the extraction procedure using distilled water and freeze-dried sediments that provoked a release of intracellular chrysolaminarin in the pool of EPS (Chiovitti et al., 2004; Takahashi et al., 2009). The optimization of extracting procedures for colloidal and bound EPS (from unfrozen sediments and with reagents that did not provoke cell lysis) could explain why the EPS did show a strong stimulation in the present experiment (Pierre et al., 2010; Takahashi et al., 2009). The proteic fraction of bound EPS was more secreted for the intermediate mud–sand mixture (M2). Zetsche et al. (2011) have shown that proteins associated with the bound EPS fraction appeared to vary with the effect of EPS on permeability, higher EPS levels leading to a decrease of sediment permeability. Lubarsky et al. (2010) have shown that protein fraction of the EPS plays a crucial role for adhesion/cohesion of the substratum but also hydrophilic properties. The higher levels of bound EPS in the intermediate mixture (M2) were probably secreted in order to decrease the permeability and to better resist to nutrient loss, thus creating a photosynthetically active biofilm. This could explain that chl a content and photosynthetic active biomass increased faster between days 3 and 6 in the intermediate mixture (M2). Proteic fraction of dowex-extracted bound EPS is involved in the pioneering stages of biofilm development (Ovain et al., 2014) and these substances are hydrophilic (Orvain et al., 2014), probably rendering the biofilm mat able to avoid losses of pore water ad associated nutrients. This phenomenon may happen for the sandier mixture (M3) too, but the duration of the experience was probably too short to observe it due to its weaker water retention.

4.2. Effect of mixture and biofilm age on erodability

Besides the biofilm age effect on sediment erodability, this study clearly put in evidence that sediment composition modifies significantly erosion resistance, with a higher $\tau_{crit\ (SPiM)}$ for the 2 mud–sand mixtures

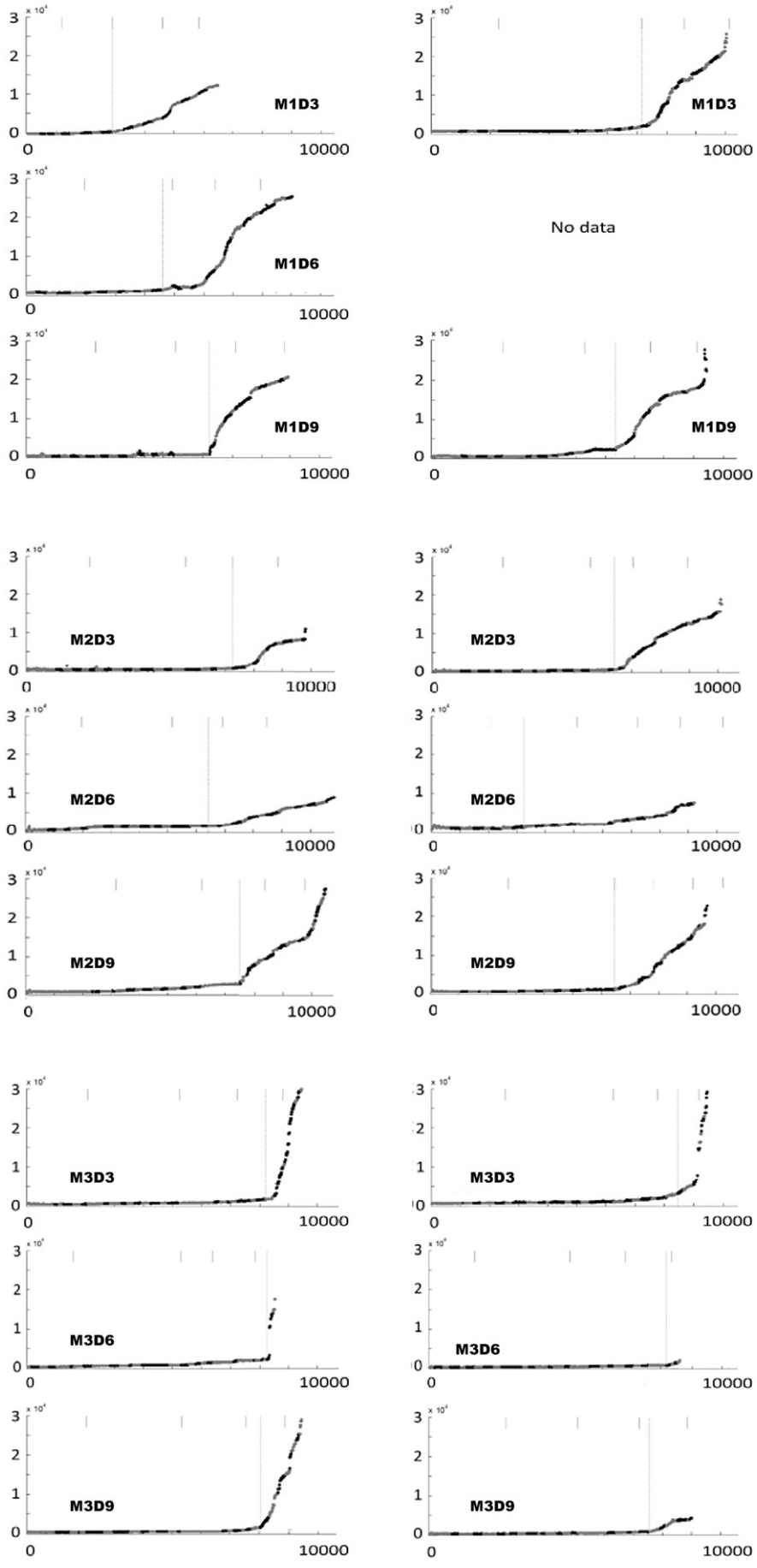
M1D3
M1D3
M1D6
No data
M1D9
M1D9
M2D3
M2D3
M2D6
M2D6
M2D9
M2D9
M3D3
M3D3
M3D6
M3D6
M3D9
M3D9
0
10000

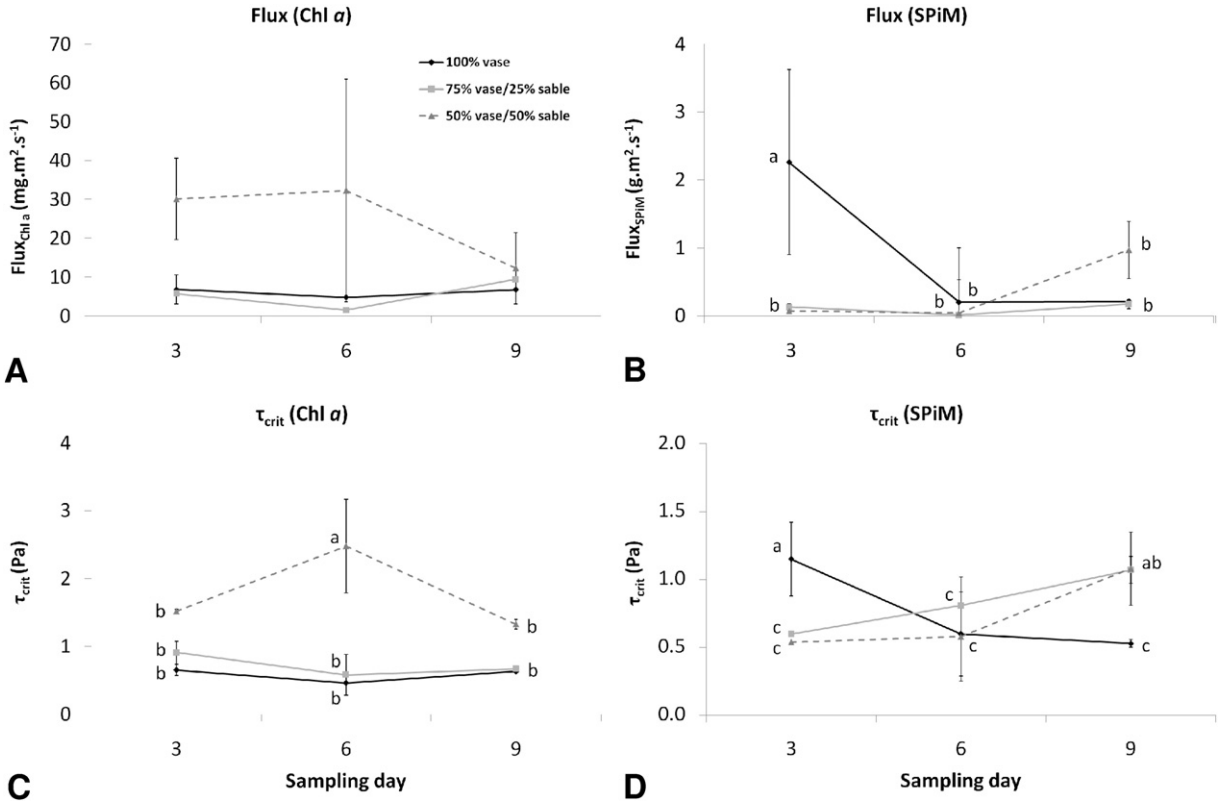

Fig. 7. Erosion features in terms of flux and crtitical erosion threshold for both Chl *a* and SPiM for the different sampling days. A: eroded flux of Chl a; B: eroded flux of SPiM; C: erosion critical threshold for Chl *a*; D: erosion critical threshold for SPiM. Letters indicate groups after post hoc test procedures (see Table 1 for further details). No significant effect was found for A and B with $\alpha = 0.05$, but M3 at days 3 and 6 for Flux(Chl *a*) differed from other values with $\alpha = 0.1$.

(M2 and M3) after 9 days of consolidation. The mud fraction therefore determines the sediment behavior and the erosion type (I for unconsolidated sediment and II for consolidated sediments). However, the erosion flux of any class of sandy or muddy types is always proportional to the mass of the mud fraction in the surface sediment. These results are in agreement with those of Mitchener and Torfs (1996), who tested 3 mud–sand mixtures (100% mud, 89% mud and 50% mud) and found that the greater sediment $\tau_{crit\ (SPiM)}$ was found for the 50% mud mixture. They estimated that the maximum $\tau_{crit\ (SPiM)}$ occurred between 30 and 50% mud content. The formula established by Ahmad et al. (2011) also confirms this observation, with a maximum in the $\tau_{crit\ (SPiM)}$ achieved at 50% of sand. Panagiotopoulos et al. (1997) found increased $\tau_{crit\ (SPiM)}$ values with greater mud fractions when adding mud to pure 152.5 μm sandy sediment from 0 to 50% mud. These results illustrate the interest of studying mixtures instead of pure mud or pure sand sediment, mixtures being able to behave like cement, thus enhancing erosion resistance or at least decreasing erodability. The dynamic bed armouring mentioned by Le Hir et al. (2011) explains the fact that the sand layer at the sediment surface is easily resuspended, but a large number of sand grains immediately settle, limiting or preventing the resuspension of underlying sediment, reducing significantly erosion rates. Thus, mud–sand mixtures (M2 and M3) may have less erosion resistance than pure cohesive sediments, but erosion rates are lower because of this dynamical bed armouring.

A significant effect of biofilm age on sediment erodability was found in this experiment in terms of critical thresholds for erosion of the two mud–sand mixtures (M2 and M3). This result is in agreement with those of Sutherland et al. (1998), Droppo et al. (2007) or Lubarsky et al. (2010), who found that the biofilm age influenced the erosion characteristics by increasing erosion threshold of SPiM during the growth stage of the biofilm. Consolidation process alone is supposed to affect positively the sediment critical erosion threshold, but the compaction effect appears mostly during the first days (Stone et al., 2008). As a consequence, the critical erosion threshold was higher at day 3 than for the other days for pure mud (M1), as observed by Lubarsky et al. (2010). The higher $\tau_{crit\ (SPiM)}$ for M1 at day 3 shows that initial lag stage must be determinant for stabilization of the bed (an increase of water content could then decrease the critical threshold). The sediment settling process probably acts in favor of the increasing $\tau_{crit\ (SPiM)}$ during the cultivation period of experiment for mixtures 2 and 3.

The carbohydrates content within the EPS colloidal fraction were well related to the water content of the sediment. Because of their solubility in water, de Winder et al. (1999) hypothesized that they may disappear as soon as the tide comes in and therefore contribute only to a limited extent to sediment stability (as clearly shown by Orvain et al., 2003a, 2003b). However, bound EPS can resist to erosion (Orvain et al, 2014) and the carbohydrates content within the EPS bound fraction may play a prominent role in the sediment grain cohesion. In this experiment, carbohydrates of the EPS bound fraction clearly explain variations in SPiM critical thresholds. The adhesion properties of carbohydrates related to the EPS bound fraction are directly responsible for biofilm establishment and better explains biostabilization of the surface sediment than colloidal EPS. Wigglesworth-Cooksey et al. (2001) confirmed that the diatom matrix extracellular carbohydrate polymer is largely responsible for sediment stabilization and that soluble polymer implied in diatom motility plays no part in the sediment stabilization process. Our results

Fig. 6. Erosion kinetics of Chl a eroded ($\mu g.m^{-2}$) as a function of time (s). M = mixture, D = day. Each curve represents a replicate of simultaneous 2 cores erosion. Water flow has been increased step by step, illustrated by the gray/black alternance on the curve. All conditions have been duplicated excepted for the mixture 1 at day 6. Water samplings have been done at $\tau = 0.166, 0.582, 1.195, 1.852$ and have been symbolized by short lines on top of the graphs (in gray). The continuous gray line corresponds to the massive erosion threshold.

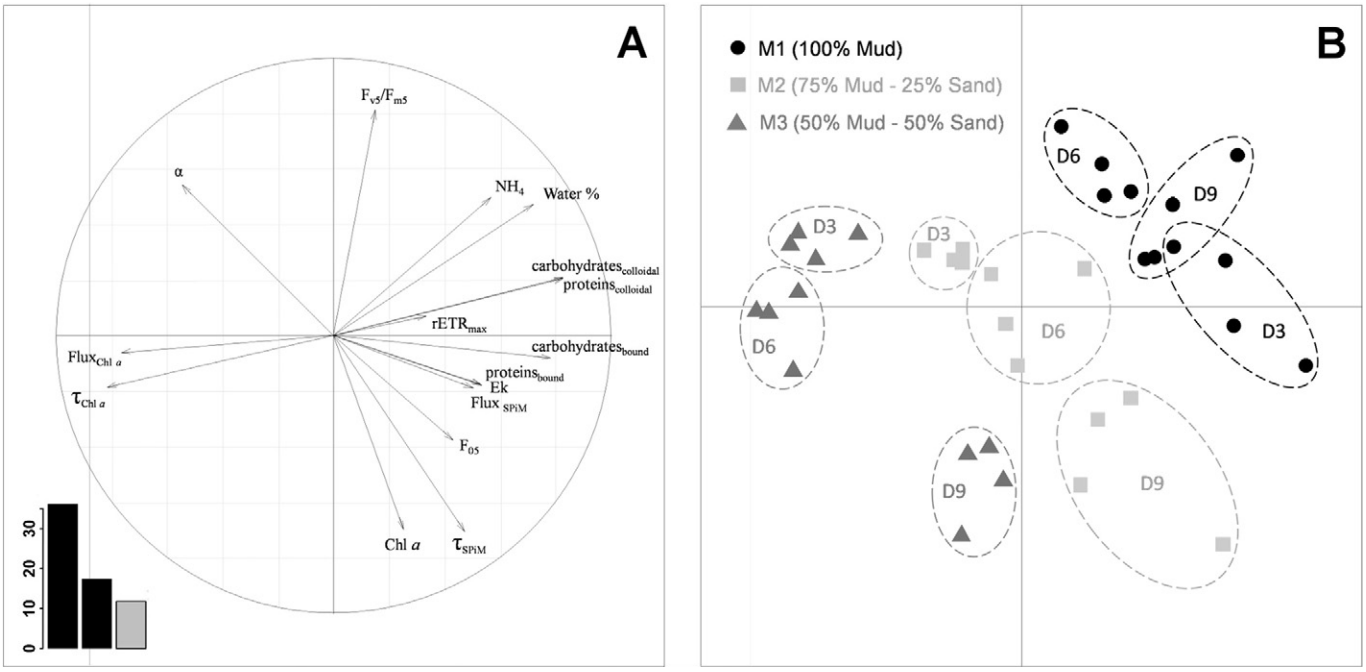

Fig. 8. Principal component analyses realized on the different biological and physical log-transformed variables. τ = critical erosion threshold, flux = mass erosion flux, SPiM = suspended particulate inorganic matter, F_{v5}/F_{m5} = physiological state of the biofilm, F_{o5} = minimum level of fluorescence, $rETR_{max}$ = maximum relative electron transport rate, NH_4 = ammonium pore water content, Ek = light saturation coefficient, water % = pore water content, Chl a = chlorophyll a content.

are in agreement with the latter, since we found that the bound carbohydrates play a predominant role in sediment erosion thresholds. The Dowex extraction allow to better target the EPS implicated in biostabilization, as shown also by Gerbersdorf et al. (2009). This EPS fraction appears to be well related to the SPiM erosion critical thresholds, with the higher concentrations corresponding to the respective higher erosion critical thresholds observed. This process allows the biofilm to colonize the sediment surface in spite of the sand presence which may impair biofilm growth.

4.3. Consequences for intertidal area functioning

Sediment mixture composition impacts biofilm shaping by providing a more or less favorable habitat for MPB, leading to differences in MPB content between mixtures. However, mixture composition seems to be the main factor involved in resuspension phenomenon, with an optimal stability reached near a equilibrate ratio between mud and sand (50/50). Pure mud allowed rapid growth of epipelic diatoms, but was also favorable to early erosion of the biomass due to the rapid formation of the biofilm and its higher fragility. Paradoxically, sand enrichment lowers the chl a erodability (higher critical bed shear stress and lower erosion flux). The formation of a biofilm in mud–sand mixtures is possible through the high production of bound EPS and its composition in proteins, which consolidates the biofilm. The mud–sand mixtures are therefore more stabilized by bound EPS than pure mud. This result is surprising, since biostabilisation exerted by MPB biofilms have been most of the time evidenced in muddy sediments. The biofilm being less well established, higher depth mass erosion is necessary to successfully pull the diatoms. The dynamic sand layer process and its protective effect evoked by Le Hir et al. (2011) have certainly explained the difficulty to erode chl a that is associated with the muddy fraction that is located deeper. Thus, a too strong sand enrichment is unfavorable to the epipelic diatom growth, as well as to their exportation to the water column via erosion. This explains well field observations made by Ubertini et al. (2012), since chl a exportation in the water column was detected in the muddiest areas of the ecosystem in Bay des Veys (Normandie, France).

On the basis of a model test regarding sediment transport, Le Hir et al. (2007, 2008) clearly showed that biostabilisation influenced by EPS is probably not a prime factor explaining the morphodynamic evolution of purely muddy areas. Most of morphodynamic changes in these habitats occur at the beginning of winter, when epipelic MPB biofilms show very low biomass and low EPS contents. By contrast, the present study put in evidence that biostabilisation effects by EPS can be very relevant, not in muddy areas, but in mud–sand mixture. This could bring many insights by explaining how MPB biofilms can develop from muddy nodal areas to surrounding areas, where substrata consist of mud–sand mixtures. These environments provide opportunities for MPB biofilm to consolidate rapidly sandy environments, when they are enriched in mud and colonized by epipelic diatoms. High content of bound EPS can provide a very efficient potential for epipelic diatoms to extend their spatial niches by reinforcing the mud enrichment, when they colonize mud–sand mixtures. In contrast to the conclusion of Le Hir et al. (2007, 2008), the pioneering role of epipelic MPB on mud enhancement along sedimentary gradients can change the basic vision of biostatilisation on intertidal mudflats. There could be a positive role of MPB owing to EPS secretion on mudflat accretion, in initial sandy environments. This effect seems to be much stronger in mud–sand mixture, and in this condition, this biotic phenomenon must influence drastically morphodynamical long-term changes by accelerating the process of extension of cohesive muddy areas to surrounding areas. These new findings must have strong implications for near-bed suspension-feeders and their habitat preferences, since mud–sand mixtures are characterized by interesting features such as its higher stability against erosion and the increased chl a exportation in the water column.

5. Conclusion

For the first time, $\tau_{crit\ (SPiM)}$ and $\tau_{crit\ (chl\ a)}$ were clearly differentiated for mud–sand mixtures. Concerning the chl a erosion, the more the sediment is rich in chl a the more the biofilm and associated chla content is resuspended quickly. Thus, the biofilm formation for pure mud resulted in an earlier detachment (with a low $\tau_{crit\ (chl\ a)}$) compared to other mixtures. Conversely, in mud–sand mixtures, the biofilm

formation is more difficult, as well as chl a erosion, happening for higher erosion thresholds. The biofilm constitutes a more labile armoring for pure mud, whereas sand enrichment increases chl a erosion thresholds. The sand vertical segregation of the sediment, along with vertical distribution of epipelic diatoms, must be the main factor responsible for the differences observed between Chl a and SPiM erosion.

In this study we aimed to clarify the respective roles of biofilm age and mixtures effect on resuspension phenomenon. Between 3 and 9 first days of biofilm development, biofilm age did significantly affect erosion critical thresholds for Chl a resuspension, and affected those of SPiM for mud–sand mixtures during biofilm growth. Proteins of the EPS bound fraction must play a critical role in the pioneering stages of biofilm installation, allowing its formation in a less favorable sand-enriched environment by increasing cohesion and lowering sediment permeability. Carbohydrate content of the bound EPS fraction was directly related to the sediment erodability, independently from mixture type or biofilm age. This reveals the relative complexity of bound EPS heteropolymers, with different properties associated to protein and carbohydrate composition of this EPS matrix.

Acknowledgments

We would like to thank the General Council of Basse-Normandie for their financial support. We would also like to thank the two anonymous reviewers for their insightful and constructive comments. **[ST]**

References

Admiraal, W., Peletier, H., Brouwer, T., 1994. The seasonal succession patterns of diatom species on an intertidal mudflat: an experimental analysis. Oikos 42, 30–40.
Ahmad, M., Dong, P., Mamat, M., 2011. The critical shear stresses for sand and mud mixture. Appl. Math. Comput. 5, 53–71.
Andersen, T.J., Pejrup, M., 2002. Biological mediation of the settling velocity of bed material eroded from an intertidal mudflat, the Danish Wadden Sea. Online 737–745.
Behrenfeld, M.J., Prasil, O., Babin, M., Bruyant, F., 2004. In search of a physiological basis for covariations in light-limited and light-saturated photosynthesis. J. Phycol. 40, 4–25.
Blanchard, G.F., Guarini, J.-M., Orvain, F., Sauriau, P.-G., 2001. Dynamic behaviour of benthic microalgal biomass in intertidal mudflats. J. Exp. Mar. Biol. Ecol. 264, 85–100.
Blanchard, G.F., Guarini, J.-M., Dang, C., Richard, P., 2004. Characterizing and quantifying photoinhibition in intertidal microphytobenthos. J. Phycol. 40, 692–696.
Bradford, M., 1976. A rapid and sensitive method for the quantitation of microgram quantities of protein using the principle of protein dye binding. Anal. Biochem. 72, 248–254.
Cartaxana, P., Ruivo, M., Hubas, C., Davidson, I., Serôdio, J., Jesus, B., 2011. Physiological versus behavioral photoprotection in intertidal epipelic and epipsammic benthic diatom communities. J. Exp. Mar. Biol. Ecol. 405, 120–127.
Chiovitti, A., Molino, P., Crawford,, S. a, Teng, R., Spurck, T., Wetherbee, R., 2004. The glucans extracted with warm water from diatoms are mainly derived from intracellular chrysolaminaran and not extracellular polysaccharides. Eur. J. Phycol. 39, 117–128.
De Brouwer, J.F.C., Wolfstein, K., Ruddy, G.K., Jones, T.E.R., Stal, L.J., 2005. Biogenic stabilization of intertidal sediments: the importance of extracellular polymeric substances produced by benthic diatoms. Microb. Ecol. 49, 501–512.
de Jonge, V.N., van Beusekom, J.E.E., 1995. Wind and tide induced resuspension of sediment and microphytobenthos from tidal flats in the Ems estuary. Limnol. Oceanogr. 40, 776–778.
De Winder, B., Staats, N., Stal, L.J., Paterson, D.M., 1999. Carbohydrate secretion by phototrophic communities in tidal sediments. 42 pp. 131–146.
Defew, E.C., Tolhurst, T.J., Paterson, D.M., Hagerthey, S.E., 2003. Can the stability of intertidal sediments be predicted from proxy parameters? An in situ investigation. 61–70. Estuarine and Coastal Sciences Association, Leamington Spa.
Droppo, I., Ross, N., Skafel, M., Liss, S., 2007. Biostabilization of cohesive sediment beds in a freshwater wave-dominated environment. Limnol. Oceanogr. 52, 577–589.
Dubois, M., Gilles, K.A., Hamilton, J.K., Rebers, P.A., Smith, F., 1956. Colorimetric method for determination of sugars and related substances. Anal. Chem. 28, 350–356.
Ehrenhauss, S., Witte, U., Janssen, F., Huettel, M., 2004. Decomposition of diatoms and nutrient dynamics in permeable North Sea sediments. Cont. Shelf Res. 24, 721–737.
Eilers, P.H.C., Peeters, J.C.H., 1988. A model for the relationship between light intensity and the rate of photosynthesis in phytoplankton. Ecol. Model. 42, 199–215.
Friend, P.L., Lucas, C.H., Holligan, P.M., Collins, M.B., 2008. Microalgal mediation of ripple mobility. Geobiology 6, 70–82.
Gerbersdorf, S.U., Jancke, T., Westrich, B., 2007. Sediment properties for assessing the erosion risk of contaminated riverine sites A comprehensive approach to evaluate sediment properties and their covariance patterns over. 7 pp. 25–35.
Gerbersdorf, S.U., Bittner, R., Lubarsky, H., Manz, W., Paterson, D.M., 2009. Microbial assemblages as ecosystem engineers of sediment stability. J. Soils Sediments 9, 640–652.
Grant, J., Bathmann, U.V., Mills, E.L., 1986. The interaction between benthic diatom films and sediment transport. Estuar. Coast. Shelf Sci. 23, 225–238.
Guizien, K., Orvain, F., Duchêne, J.-C., Le Hir, P., 2012. Accounting for rough bed friction factors of mud beds due to biological activity in erosion experiments. J. Hydraul. Eng. 138, 979–984.
Holland, A.F., Zingmark, R.G., Dean, J.M., 1974. Quantitative evidence concerning the stabilization of sediments by marine benthic diatoms. Mar. Biol. 27, 191–196.
Holmes, R.M., Aminot, A., Kérouel, R., Hooker, B.A., Peterson, B.J., 1999. A simple and precise method for measuring ammonium in marine and freshwater ecosystems. Can. J. Fish. Aquat. Sci. 56, 1801–1808.
Jesus, B., Brota, V., Marani, M., Paterson, D.M., 2005. Spatial dynamics of microphytobenthos determined by PAM fluorescence. Estuar. Coast. Shelf Sci. 65, 30–42.
Krantzberg, G., 1985. The influence of bioturbation on physical, chemical and biological parameters in aquatic environments: a review. Environ. Pollut. A, Ecol. Biol. 39, 99–122.
Le Hir, P., Monbet, Y., Orvain, F., 2007. Sediment erodability in sediment transport modelling: can we account for biota effects? Cont. Shelf Res. 27, 1116–1142.
Le Hir, P., Canna, P., Waelesb, B., Jestina, H., Bassoulleta, P., 2008. Erodibility of natural sediments: experiments on sand/mud mixtures from laboratory and field erosion tests. Proceedings in Marine Science 9, 137–153.
Le Hir, P., Cayocca, F., Waeles, B., 2011. Dynamics of sand and mud mixtures: a multiprocess-based modelling strategy. Cont. Shelf Res. 31, S135–S149.
Lefebvre, S., Mouget, J.-L., Lavaud, J., 2011. Duration of rapid light curves for determining in situ the photosynthesis of microphytobenthos biofilm. Aquat. Bot. 95, 1–8.
Lelieveld, S., Pilditchb, C.A., Green, M.O., 2003. Variation in sediment stability and relation to indicators of microbial abundance in the Okura Estuary, New Zealand. Estuar. Coast. Shelf Sci. 57, 123–136.
Lorenzen, C.J., 1967. Determination of chlorophyll and phaeopigments: spectrophotometric equations. Limnol. Oceanogr. 343–346.
Lubarsky, H.V., Hubas, C., Chocholek, M., Larson, F., Manz, W., Paterson, D.M., Gerbersdorf, S.U., 2010. The stabilisation potential of individual and mixed assemblages of natural bacteria and microalgae. PLoS ONE 5, e13794.
Lucas, C.H., 2003. Observations of resuspended diatoms in the turbid tidal edge. J. Sea Res. 50, 301–308.
MacIntyre, H.L., Kana, T.M., Anning, T., Geider, R.J., 2002. Photoacclimation of photosynthesis irradiance response curves and photosynthetic pigments in microalgae and cyanobacteria. J. Phycol. 38, 17–38.
McKew, B.A., Taylor, J.D., McGenity, T.J., Underwood, G.J., 2011. Resistance and resilience of benthic biofilm communities from a temperate saltmarsh to desiccation and rewetting. ISME J. 5, 1–30.
Migniot, C., 1989. Tassement et rhéologie des vases, 1ère partie. La Houille Blanche 1, 11–29.
Mitbavkar, S., Anil, A., 2004. Vertical migratory rhythms of benthic diatoms in a tropical intertidal sand flat: influence of irradiance and tides. Mar. Biol. 145, 9–20.
Mitchener, H., Torfs, H., 1996. Erosion of mud/sand mixtures. Coast. Eng. 29, 1–25.
Morris, E.P., 2005. Quantifying Primary Production Of Microphytobenthos: Application Of Optical Methods. Univ. Groningen.
Orvain, F., Galois, R., Barnard, C., 2003a. Carbohydrate production in relation to microphytobenthic biofilm development: an integrated approach in a tidal mesocosm. Microb. Ecol. 45, 237–251.
Orvain, F., Le Hir, P., Sauriau, P., 2003b. A model of fluff layer erosion and subsequent bed erosion in the presence of the bioturbator, *Hydrobia ulvae*. J. Mar. Res. 61, 823–851.
Orvain, F., Sauriau, P.G., Sygut, A., Joassard, L., Le Hir, P., 2004. Interacting effects of *Hydrobia ulvae* bioturbation and microphytobenthos on the erodibility of mudflat sediments. Mar. Ecol. Prog. Ser. 278, 205–223.
Orvain, F., Lefebvre, S., Montepini, J., Sébire, M., Gangnery, A., Sylvand, B., 2012. Spatial and temporal interaction between sediment and microphytobenthos in a temperate estuarine macro-intertidal bay. Mar. Ecol. Prog. Ser. 458, 53–68.
Orvain, F., De Crignis, M., Guizien, K., Lefebvre, S., Mallet, C., Takahashi, E., Dupuy, C., 2014. Tidal and seasonal effects on the consortium of bacteria, microphytobenthos and exopolymers in natural intertidal biofilms (Brouage, France). J. Sea Res. 92, 6–18.
Paarlberg, a, Knaapen, M., Devries, M., Hulscher, S., Wang, Z., 2005. Biological influences on morphology and bed composition of an intertidal flat. Estuar. Coast. Shelf Sci. 64, 577–590.
Panagiotopoulos, I., Voulgaris, G., Collins, M.B., 1997. The influence of clay on the threshold of movement of fine sandy beds. Coast. Eng. 32, 19–43.
Parkhill, J.P., Maillet, G., Cullen, J.J., 2001. Fluorescence-based maximal quantum yield for PSII as a diagnostic of nutrient stress. Journal of Phycology 37, 517–529.
Paterson, D.M., 1989. Short-term changes in the erodibility of intertidal cohesive sediments related to the migratory behaviour of epipelic diatoms. Limnol. Oceanogr. 34, 223–234.
Perkins, R., 2003. Changes in microphytobenthic chlorophyll a and EPS resulting from sediment compaction due to de-watering: opposing patterns in concentration and content. Cont. Shelf Res. 23, 575–586.
Perkins, R.G., Underwood, G.J.C., Brotas, V., Snow, G.C., Jesus, B., Ribeiro, L., 2001. Responses of microphytobenthos to light: primary production and carbohydrate allocation over an emersion period. Mar. Ecol. Prog. Ser. 223, 101–112.
Pierre, G., Graber, M., Orvain, F., Dupuy, C., Maugard, T., 2010. Biochemical characterization of extracellular polymeric substances extracted from an intertidal mudflat using a cation exchange resin. Biochem. Syst. Ecol. 38, 917–923.
Saburova, M.A., Polikarpov, I.G., 2003. Diatom activity within soft sediments: behavorial and physiological processes. Mar. Ecol. Prog. Ser. 251, 115–126.
Serôdio, J., 2003. A chlorophyll fluorescence index to estimate short-term rates of photosynthesis by intertidal microphytobenthos. J. Phycol. 39, 33–46.
Serôdio, J., Vieira, S., Cruz, S., Barroso, F., 2005. Short-term variability in the photosynthetic activity of microphytobenthos as detected by measuring rapid light curves using variable fluorescence. Mar. Biol. 146, 903–914.

Serôdio, J., Vieira, S., Cruz, S., 2008. Photosynthetic activity, photoprotection and photoinhibition in intertidal microphytobenthos as studied in situ using variable chlorophyll fluorescence. Cont. Shelf Res. 28, 1363–1375.
Smith, D., Underwood, G., 1998. Exopolymer production by intertidal epipelic diatoms. Limnol. Oceanogr. 43, 1578–1591.
Smith, D., Underwood, G., 2001. The production of extracellular carbohydrates by estuarine benthic diatoms: the effects of growth phase and light and dark treatment. J. Phycol. 333, 321–333.
Spears, B., Saunders, J., 2008. Microalgal sediment biostabilisation along a salinity gradient in the Eden Estuary, Scotland: unravelling a paradox. Mar. Freshwat. Res. 59, 313–321.
Staats, N., Stal, L., Mur, L., 2000a. Exopolysaccharide production by the epipelic diatom *Cylindrotheca closterium*: effects of nutrient conditions. J. Exp. Mar. Biol. Ecol. 249, 13–27.
Staats, N., Stal, L.J., De Winder, B., Mur, L.R., 2000b. Oxygenic photosynthesis as driving process in exopolysaccharide production of benthic diatoms. Mar. Ecol. Prog. Ser. 193, 261–269.
Stone, M., Krishnappan, B.G., Emelko, M.B., 2008. The effect of bed age and shear stress on the particle morphology of eroded cohesive river sediment in an annular flume. Water Res. 42, 4179–4187.
Sutherland, T.F., Amos, C.L., Grant, J., 1998. The effect of carbohydrate production by the diatom *Nitzschia curvilineata* on the erodibility of sediment. Limnol. Oceanogr. 43, 65–72.
Takahashi, E., Ledauphin, J., Goux, D., Orvain, F., 2009. Optimising extraction of extracellular polymeric substances (EPS) from benthic diatoms: comparison of the efficiency of six EPS extraction methods. Mar. Freshwat. Res. 1–10.
Tolhurst, T.J., Jesus, B., Brotas, V., Paterson, D.M., 2003. Diatom migration and sediment armouring — an example from the Tagus Estuary, Portugal. Mar. Ecol. 183–193.
Tolhurst, T.J., Defew, E.C., Brouwer, J.F.C. De, Wolfstein, K., 2006. Small-scale temporal and spatial variability in the erosion threshold and properties of cohesive intertidal sediments. Cont. Shelf Res. 26, 351–362.
Tolhurst, T.J., Watts, C.W., Vardy, S., Saunders, J.E., Consalvey, M.C., Paterson, D.M., 2008. The effects of simulated rain on the erosion threshold and biogeochemical properties of intertidal sediments. Cont. Shelf Res. 28, 1217–1230.
Ubertini, M., Lefebvre, S., Gangnery, A., Grangere, K., Le Gendre, R., Orvain, F., 2012. Spatial variability of benthic-pelagic coupling in an estuary ecosystem: consequences for microphytobenthos resuspension phenomenon. Plos ONE 7, 1–17.
Underwood, G., Smith, D., 1998. Predicting epipelic diatom exopolymer concentrations in intertidal sediments from sediment chlorophyll a. Microb. Ecol. 35, 116–125.
Van de Koppel, J., Herman, P., Thoolen, P., Heip, C., 2001. Do alternate stable states occur in natural ecosystems? Evidence from a tidal flat. Ecology 82, 3449–3461.
Waeles, B., Hir, P. Le, Lesueur, P., 2008. Sediment and ecohydraulics. INTERCOH 2005. Elsevier.
Wigglesworth-Cooksey, B., Berglund, D., Cooksey, K.E., 2001. Cell–cell and cell–surface interactions in an illuminated biofilm: implications for marine sediment stabilization. Geochem. Trans. 2, 75.
Wolf, G., 2007. Kinetic modeling of phototrophic biofilms: the PHOBIA model. Biotechnol. Bioeng. 97, 1064–1079.
Yallop, M., Paterson, D., Wellsbury, P., 2000. Interrelationships between rates of microbial production, exopolymer production, microbial biomass, and sediment stability in biofilms of intertidal sediments. Microb. Ecol. 39, 116–127.
Zetsche, E., Paterson, D., Lumsdon, D., Witte, U., 2011. Temporal variation in the sediment permeability of an intertidal sandflat. Mar. Ecol. Prog. Ser. 441, 49–63.
Ziervogel, K., Forster, S., 2006. Do benthic diatoms influence erosion thresholds of coastal subtidal sediments? J. Sea Res. 55, 43–53.